

SUBARU MID-INFRARED IMAGING OF THE QUADRUPLE LENSES. II. UNVEILING LENS STRUCTURE OF MG0414+0534 AND Q2237+030¹TAKEO MINEZAKI², MASASHI CHIBA³, NOBUNARI KASHIKAWA⁴, KAIKI TARO INOUE⁵, AND HIROKAZU KATAZA⁶*To appear in the Astrophysical Journal*

ABSTRACT

We present mid-infrared imaging at 11.7 μm for the quadruple lens systems, MG0414+0534 and Q2237+030, using the cooled mid-infrared camera and spectrometer (COMICS) attached on the Subaru telescope. MG0414+0534 is characterized by a bright pair of lensed images (A1, A2) and their optical flux ratio A2/A1 deviates significantly from the prediction of a smooth lens model. Q2237+030 is “the Einstein cross” being comprised of four lensed images, which are significantly affected by microlensing in a foreground lensing galaxy. Our mid-infrared observations of these lensed images have revealed that the mid-infrared flux ratio for A2/A1 of MG0414+0534 is nearly unity (0.90 ± 0.04). We find that this flux ratio is systematically small, at 4 to 5 σ level, compared with the prediction of a best smooth lens model (1.09) represented by a singular isothermal ellipsoid and external shear. The smooth lens model which also considers the additional lensing effect of the possible faint satellite, object X, provides yet a large flux ratio of A2/A1 = 1.06, thereby suggesting the presence of more substructures to explain our observational result. In contrast, for Q2237+030, our high signal-to-noise observation indicates that the mid-infrared flux ratios between all the four images of Q2237+030 are virtually consistent with the prediction of a smooth lens model. Based on the size estimate of the dust torus surrounding the nuclei of these QSOs, we set limits on the mass of a substructure in these lens systems, which can cause anomalies in the flux ratios. For MG0414+0534, since the required mass of a substructure inside its Einstein radius is $\gtrsim 360 M_{\odot}$, millilensing by a CDM substructure is most likely. If it is modeled as a singular isothermal sphere, the mass inside radius of 100 pc is given as $\gtrsim 1.0 \times 10^5 M_{\odot}$. For Q2237+030, there is no significant evidence of millilensing, so the reported anomalous flux ratios in shorter wavelengths are entirely caused by microlensing by stars.

Subject headings: gravitational lensing — infrared: galaxies — quasars: individual (MG0414+0534, Q2237+030)

1. INTRODUCTION

Although the cold dark matter (CDM) scenario is now a leading theoretical paradigm for understanding the formation of large-scale structures in the Universe, it confronts yet various discrepancies with observations on smaller, galactic and sub-galactic scales. One of the most serious issues is so-called “the missing satellites problem”, namely, while the total number of known Milky Way satellites is about twenty, CDM models predict the existence of more than several hundred substructures of dark matter or “CDM subhalos” with masses of $M \sim 10^7\text{--}10^9 M_{\odot}$, in a galaxy-sized halo with $M \sim 10^{12} M_{\odot}$ (Klypin et al. 1999; Moore et al. 1999; see also Diemand et al. 2007 for more recent, high resolution studies). The abundance of CDM halos on small scales is closely relevant to the small-scale power spectrum of initial density fluctuations, thereby affecting the formation

of the first generation objects and the resultant reionization history of the Universe. Also, their abundance in a galaxy-sized halo reflects the merging history and dynamical evolution of dark-matter halos in the expanding Universe, thereby being associated with the formation of luminous galaxies within the framework of hierarchical galaxy formation scenarios.

To clarify this outstanding issue, gravitational lensing offers us an invaluable insight into the spatial structure of a galaxy-sized dark halo, which works as a lens for a remote source, such as a QSO. In particular, flux ratios between multiple images of a lensed source are a sensitive probe for the mass distribution of a lens. There exist a class of lensed QSOs having anomalous flux ratios, namely, those hardly reproduced by any lens models with a smooth density distribution and such flux anomalies can be caused by any substructures that reside in a lensing galaxy through either of *millilensing* by CDM subhalos or *microlensing* by stellar objects (e.g., Mao & Schneider 1998; Metcalf & Madau 2001; Chiba 2002).

For the purpose of enlightening the nature of lens substructures, mid-infrared observations of lensed images and their flux ratios provide us with advantageous perspectives compared with the studies in other wavelengths. Firstly, mid-infrared flux is free from extinction effects. The extinction by intervening dust working differentially on each lensed image does not affect flux ratios in mid-infrared band, contrary to optical flux ratios. Secondly, mid-infrared flux is free from microlensing effects.

¹ Based on data collected at Subaru Telescope, which is operated by the National Astronomical Observatory of Japan.

² Institute of Astronomy, School of Science, University of Tokyo, Mitaka, Tokyo 181-0015, Japan; minezaki@ioa.s.u-tokyo.ac.jp

³ Astronomical Institute, Tohoku University, Aoba-ku, Sendai 980-8578, Japan; chiba@astr.tohoku.ac.jp

⁴ National Astronomical Observatory, Mitaka, Tokyo 181-8588, Japan; n.kashikawa@nao.ac.jp

⁵ School of Science and Engineering, Kinki University, Higashi Osaka 577-8502, Japan; kinoue@phys.kindai.ac.jp

⁶ Institute of Space and Astronautical Science, Japan Aerospace Exploration Agency, Sagami-hara, Kanagawa 229-8510, Japan; kataza@ir.isas.jaxa.jp

Observed mid-infrared flux originates basically from the dust torus of a QSO producing near-infrared emission at the rest frame. The torus is so spatially extended, with a radius of ~ 1 pc, that its flux is unaffected by stars in the foreground lensing galaxy (microlensing) because their Einstein radii are only ~ 0.01 pc. On the other hand, CDM subhalos having much larger Einstein radii (millilensing) can affect the mid-infrared flux from a dust torus. Finally, the inner radius of a dust torus surrounding a central engine can quantitatively be estimated from the QSO luminosity, based on the technique of dust reverberation observations (Minezaki et al. 2004). Then making use of an available source size for this lensing event, it is possible to place a useful limit on the mass of CDM subhalos. In this regard, mid-infrared observations are more advantageous than radio ones, because of the availability of a source size for both radio-loud and radio-quiet QSOs.

This is the second paper reporting our series of mid-infrared observations of quadruple lenses with anomalous optical flux ratios, using the Subaru telescope. Our first paper dedicated to PG1115+080 and B1422+231 was published in Chiba et al. (2005, hereafter referred to as Paper I). Here we report the results of two quadruple lenses MG0414+0534 and Q2237+030, which were discovered by Hewitt et al. (1992) and Huchra et al. (1985), respectively.

MG0414+0534 is located at a source redshift of $z_S = 2.639$ and lensed by a foreground elliptical galaxy at a redshift of $z_L = 0.9584$ (Lawrence et al. 1995; Tonry & Kochanek 1999). This lens system consists of four lensed images referred to as A1, A2, B, and C, with the separation between a close pair of bright images A1 and A2 being $\sim 0.''4$. This image configuration of A1 and A2 emerges if the QSO is close to and inside a fold caustic provided by the foreground lens and the flux ratio between both images is expected to be unity for an ideally smooth lens. In MG0414+0534, this flux ratio has been observed to be a function of wavelength, where A2 is found to be fainter than A1, and this has been interpreted as a result of differential extinction in the lens and/or of microlensing of one or more of the images (e.g., Lawrence et al. 1995; Malhotra, Rhoads, & Turner 1997; Falco et al. 1997; McLeod et al. 1998; Tonry & Kochanek 1999; Angonin-Willaime et al. 1999; Ros et al. 2000).

Q2237+030 is located at $z_S = 1.695$ and lensed by the central bulge component of a foreground spiral galaxy at $z_L = 0.0394$ (Huchra et al. 1985). This is the famous Einstein Cross consisting of four images A, B, C, and D. It has been known that these lensed images as measured in optical wavelengths are strongly affected by microlensing, so that the optical flux ratios between lensed images differ from the predictions of a smooth lens (Irwin et al. 1989). Agol, Jones, & Blaes (2000) observed this system in mid-infrared using the Keck telescope and reported that the mid-infrared flux ratios may be explained by a smooth lens model within the limitation of their data having intermediate S/N ratios (see also Agol et al. 2001). Metcalf et al. (2004) performed an integral-field spectroscopy of this system and showed that the emission-line flux ratios such as those of $[O_{III}]$ may suggest some signature of lens substructures. Thus, further independent studies based on mid-infrared observations of both systems are required to deduce the nature of their

anomalous flux ratios.

The paper is organized as follows. In §2, we show the observations of our current targets. In §3, the procedure of data reduction is presented to obtain the mid-infrared fluxes and their ratios among the lensed images. In §4, the implications for the current observational results are discussed and the conclusions are drawn in §5. In what follows, we adopt the set of cosmological parameters of $\Omega = 0.3$, $\Lambda = 0.7$, and $h = 0.7$ ($h \equiv H_0/100$ km s $^{-1}$ Mpc $^{-1}$) for all relevant estimations, as adopted in Paper I.

2. OBSERVATION

The mid-infrared imaging of MG0414+0534 and Q2237+030 was carried out on 2005 October 10 and 11 (UT), using the cooled mid-infrared camera and spectrometer (COMICS; Kataza et al. 2000) attached on the Cassegrain focus of the Subaru telescope. The field of view is $42'' \times 32''$ and the pixel scale is $0.''129$ pixel $^{-1}$. We used the N11.7 filter, whose effective wavelength and bandwidth are $\lambda_c = 11.67$ μ m and $\Delta\lambda = 1.05$ μ m, respectively. The chopping frequency was set 0.45 Hz with a width of $10''$, and in addition to the chop, the telescope position was dithered during the observation. The FWHM of point-spread function (PSF) was about $0.''33$, and the diffraction core was seen in the PSF. The total exposure times of the available data were 3.2 hours for MG0414+0534 and 5.8 hours for Q2237+030, respectively. The nights were photometric during the observation, and HD25477 and HD206445 were observed for the photometric standard stars (Cohen et al. 1999).

The images were reduced in the same way as described in detail in Paper I. The resultant mid-infrared ($\lambda = 11.7$ μ m) images of the lensed QSOs, MG0414+0534 and Q2237+030, are presented in Figure 1. The images presented in the figure have been re-sampled with half size of pixels (the pixel scale is $0.''065$ pixel $^{-1}$). They also have been smoothed with a Gaussian kernel of $\sigma_r = 0.''065$ in order to improve their visual impression, although photometries were carried out based on the images without any smoothing. As presented in Figure 1, the lensed images A1 and A2 of MG0414+0534 and all lensed images of Q2237+030 were clearly detected and well separated from each other. The faint lensed images B and C of MG0414+0534 were also detected.

3. RESULTS

The fluxes and the flux ratios of the lensed images of MG0414+0534 and Q2237+030 were derived as described in Paper I.

The fluxes of $f(A1+A2)$ of MG0414+0534 and $f(A+B+D)$ of Q2237+030 were measured by aperture photometry, then the total fluxes of all lensed images were estimated from the aperture-photometry fluxes and the flux ratios obtained as described later, because the images B, C of MG0414+0534 and the image C of Q2237+030 were much fainter than the others. Since the lensed images were so close each other, the fluxes of $f(A1+A2)$ of MG0414+0534 and $f(A+B+D)$ of Q2237+030 were measured by connecting the circular apertures of $1.''3$ in diameter for each lensed image. The amounts of aperture corrections were estimated by calculating the flux losses of the photometric apertures for MG0414+0534 and Q2237+030 respectively, based

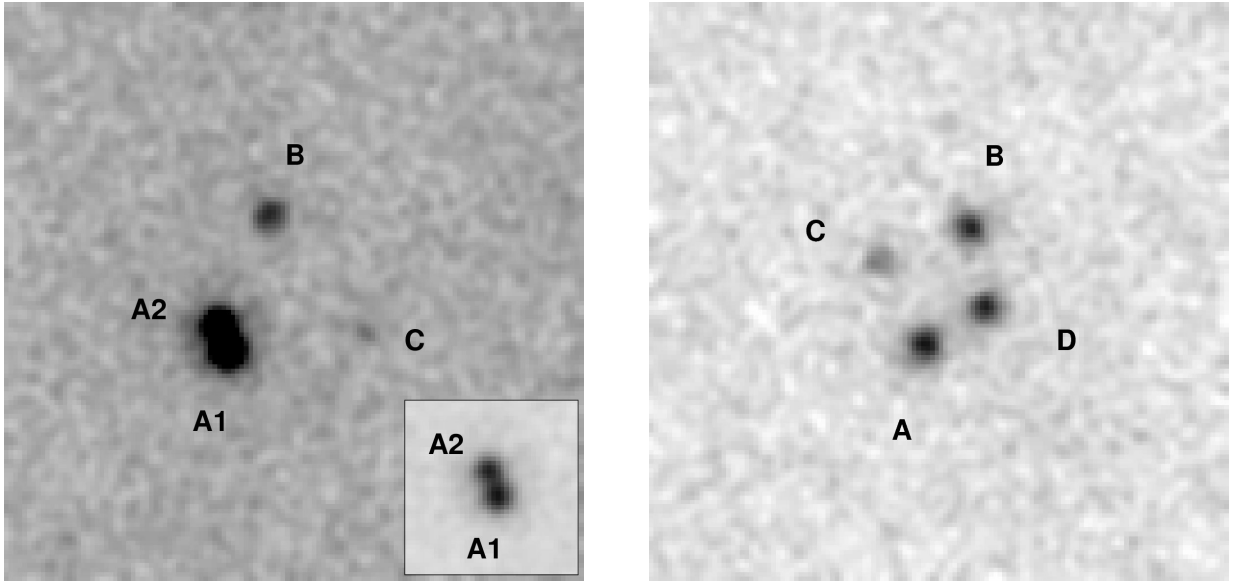


FIG. 1.— Quadruple lens systems MG0414+0534 (left) and Q2237+030 (right) at $11.7\ \mu\text{m}$ taken with COMICS/Subaru on 2005 October 10 and 11 (UT). *Inset (left)*: Image A1 and A2 of MG0414+0534 in a different level of grayscale. North is up, east is left, and the pixel scale of them is $0.''065\ \text{pixel}^{-1}$. These images have been smoothed with a Gaussian kernel of $\sigma = 0.''065$ in order to improve their visual impression.

on the growth curve of flux within circular apertures (from $0.''5$ to $4.''6$ in diameter) derived from the multi-aperture photometry of the photometric standard stars. They were estimated as about 10% and corrected. The fluxes of the lensed QSOs were calibrated by comparing the fluxes of the photometric standard stars, HD25477 and HD206445, whose fluxes were calculated by integrating its spectral energy distribution (SED) presented by Cohen et al. (1999) with the top-hat function of $\lambda_c = 11.67\ \mu\text{m}$ and $\Delta\lambda = 1.05\ \mu\text{m}$.

The flux ratios between the lensed images were estimated by PSF-fitting photometry, with the fitting aperture of $1.''3$ in diameter. The PSF was modeled by a circular Gaussian radial profile for Q2237+030. On the other hand, the PSF was modeled by a circular double Gaussian profile for MG0414+0534, in order to fit the diffraction-core plus extended-tail profile seen in its lensed images. The relative positions between the images were taken from the CASTLES web site⁷ (based on the *Hubble Space Telescope* (HST) imaging observations). The free parameters of the fit were the fluxes of the lensed images, the positional shift of the whole images, and the widths of the model PSFs. We first fitted only the bright lensed images (A1, A2 of MG0414+0534, A, B, D of Q2237+030), then fitted the remaining images with only the parameters of their fluxes being free.

The errors of the fluxes and the flux ratios were estimated by the following simulation, because they were determined not only by photon statistics and detector noise, but also by the fluctuation of very high sky-background in mid-infrared imaging observation, which remains even after the image reduction process. Here we note that the final image of MG0414+0534 was obtained by summing 114 reduced images with an exposure time of 100 s, and that of Q2237+030 was obtained by summing 210 reduced images. First, eight independent

blank-sky areas of $8.3'' \times 8.3''$ were selected surrounding the target in each of the reduced image with an exposure time of 100 s. Secondly, the artificial image of the target was added to those blank-sky areas. It was modeled according to the results of the aperture and the PSF-fitting photometries: the flux of each lensed image of the target was determined by the aperture-photometry flux and the best-fit flux ratios obtained by the PSF-fitting photometry, and the radial profile of each lensed image was a circular double Gaussian profile for MG0414+0534, or a circular Gaussian profile for Q2237+030, with the best-fit widths of the model PSF. Thirdly, those “artificial target plus blank-sky” images were summed in the same way as did for the real data (summing 114 images for MG0414+0534 and 210 images for Q2237+030) to obtain eight artificial final images. Finally, the aperture and the PSF-fitting photometries were applied to them in the same way as did for the real data to measure the fluxes and the flux ratios. Then, the standard deviations of them were calculated to estimate the errors of the flux and the flux ratios.

The fluxes, the flux ratios, and their $1\ \sigma$ errors of MG0414+0534 and Q2237+030 are listed in Table 1 and 2. For comparison, the flux ratios in various wavelengths reported in the literature and the prediction of the smooth lens models (will be described in the next section) are listed in Table 3 and 4. We obtained the mid-infrared flux ratios of MG0414+0534 for the first time, and obtained the most precise measurements of those of Q2237+030. These properties in the flux ratios of both lens systems provide important implications for the nature of lens substructure, as discussed in the next section.

4. DISCUSSION

4.1. Flux Ratios Predicted by a Lens Model

⁷ <http://cfa-www.harvard.edu/glensdata/>

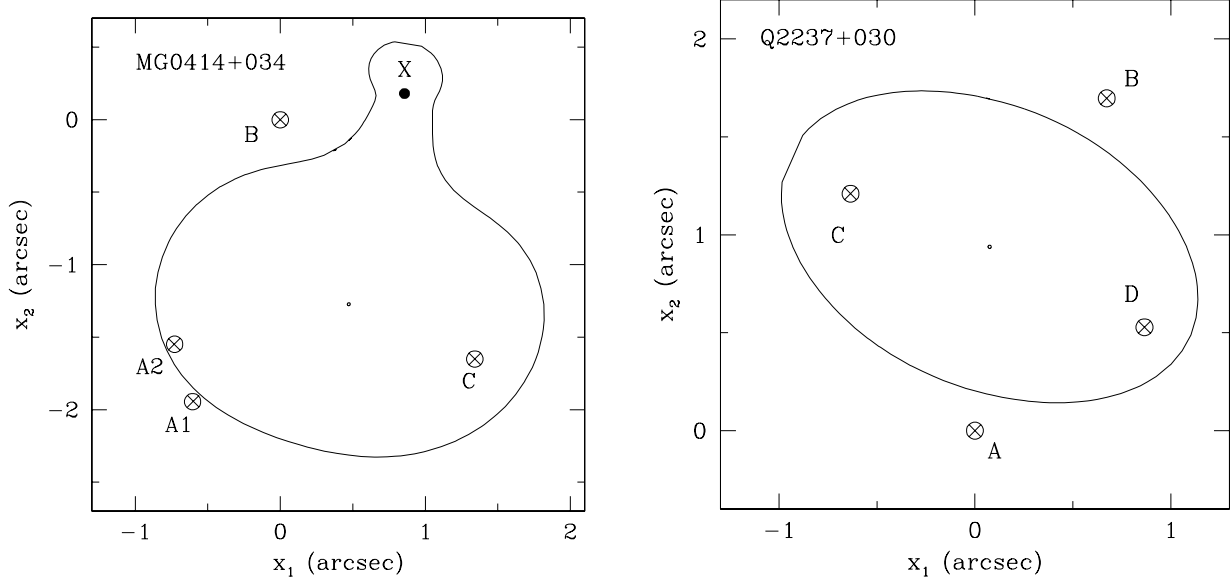


FIG. 2.— The best-fit model (SIE+ES+X) for MG0414+0534 (left) and that (SIE+ES) for Q2237+030 (right). For MG0414+0534, the lensing effect of a possible faint satellite (object X) is taken into account as explained in the text. Crosses show the observed positions of images, whereas open circles show the best-fit positions of the images in the lens models. Solid lines denote the critical curves.

TABLE 1
MID-INFRARED FLUX AND FLUX RATIO OF MG0414+0534

| flux | flux | flux ratio | | |
|----------------|----------------|-----------------|-----------------|-----------------|
| A1+A2 | All | A2/A1 | B/A1 | C/A1 |
| (mJy) | (mJy) | | | |
| 31.2 ± 1.0 | 39.2 ± 1.4 | 0.90 ± 0.04 | 0.36 ± 0.02 | 0.12 ± 0.03 |

TABLE 2
MID-INFRARED FLUX AND FLUX RATIO OF Q2237+030

| flux | flux | flux ratio | | |
|----------------|----------------|-----------------|-----------------|-----------------|
| A+B+D | All | B/A | C/A | D/A |
| (mJy) | (mJy) | | | |
| 19.0 ± 0.9 | 22.2 ± 1.0 | 0.84 ± 0.05 | 0.46 ± 0.02 | 0.87 ± 0.05 |

The configuration of these quadruple lens systems can be reproduced by an elliptical lens. We here select a singular isothermal ellipsoid (SIE) plus an external shear if required (SIE+ES) (Kormann, Schneider, & Bartelmann 1994) as a fiducial smooth lens model. The model is a simple but sufficient representation for highlighting the general properties of many smooth lens models which have been constructed for reproducing these lens systems. The current model holds the following parameters: the critical angular scale (Einstein radius in an angular scale) characterizing the strength of the lens potential b , the ellipticity e of the lens and its position angle θ_e , the strength and direction of the external shear (γ, θ_γ), and the lens galaxy position on the lens plane (x_0, y_0). The basic observational constraints are the (relative) positions of the lensed images and lensing galaxy. Regarding the observed mid-infrared flux ratios, we use them only for the composite lens models of MG0414+0534 (i.e., considering an additional faint satellite and/or mul-

tipoles as introduced later), so that the models are not under-constrained by observations. We adopt the positional data from the CASTLES web site for both systems. For MG0414+0534 (Q2237+030), the positions relative to image B (image A) are measured with an error of $0.''003$ ($0.''003$) for lensed images and $0.''003$ ($0.''004$) for a lens galaxy. We use the LENSMODEL package developed by Keeton (2001) to find the solutions for the image positions and undertake the χ^2 fitting to find the best model parameters, which are generally in good agreement with previous models. Table 5 summarizes the best model parameters and flux ratios predicted by the current smooth lens model. Figure 2 shows the configuration of the best-fit lens models for MG0414+0534 (left, including the effect of a faint satellite as explained below) and Q2237+030 (right). Detailed model results for each lensing system are explained in the following.

4.1.1. MG0414+0534

For this quadruple lens, an SIE alone yields a very large χ^2/N_{dof} of ~ 400 with $N_{\text{dof}} = 3$, so the inclusion of an external shear (SIE+ES) is important for decreasing χ^2 significantly as listed in the table. However, this model yields still a large χ^2 to accept as the best model, where some degeneracies between e and γ exist. We further consider the lensing effect of a possible faint satellite, object X (Schechter & Moore 1993), as has been adopted in the previous lens models (e.g., Ros et al. 2000). For this additional component of the lens, we assume a singular isothermal sphere (SIS) with an optimized Einstein angle b_X , where the lens position is $(x_X, y_X) = (0.''857, 0.''180)$ with an error of $0.''010$ as taken from the CASTLES web site. The object X is assumed to be at the same redshift as the lensing galaxy. We include these three parameters of object X in our lens fitting procedure: this model is referred to as SIE+ES+X, yielding a statistically reasonable fit to the image positions. In addition, we consider

TABLE 3
FLUX RATIOS OF MG0414+0534

| wavelength | date | A2/A1 | flux ratio B/A1 | C/A1 | reference |
|----------------------------|----------------|---------------------|---------------------|---------------------|-----------|
| F814W (0.8 μm) | | 0.425 ± 0.033 | 0.474 ± 0.040 | 0.215 ± 0.018 | 1 |
| F110W (1.1 μm) | | 0.637 ± 0.024 | 0.417 ± 0.016 | 0.194 ± 0.007 | 1 |
| F160W (1.6 μm) | | 0.738 ± 0.025 | 0.391 ± 0.013 | 0.179 ± 0.005 | 1 |
| F205W (2.1 μm) | | 0.832 ± 0.017 | 0.384 ± 0.015 | 0.174 ± 0.002 | 1 |
| 22 GHz | 1994.04.01 | 0.881 ± 0.013 | 0.397 ± 0.004 | 0.157 ± 0.003 | 2 |
| 15 GHz | 1993.01.15 | 0.8905 ± 0.0049 | 0.3896 ± 0.0015 | 0.1515 ± 0.0013 | 2 |
| 8 GHz | 1993.01.15 | 0.8974 ± 0.0016 | 0.3887 ± 0.0005 | 0.1492 ± 0.0004 | 2 |
| 5 GHz | 1993.01.15 | 0.898 ± 0.010 | 0.386 ± 0.003 | 0.144 ± 0.002 | 2 |
| 11.7 μm | 2005.10.11, 12 | 0.90 ± 0.04 | 0.36 ± 0.02 | 0.12 ± 0.03 | 3 |
| SIE+ES | | 1.090 | 0.257 | 0.107 | 4 |
| SIE+ES+X | | 1.063 | 0.321 | 0.158 | 4 |

NOTE. — The references are 1: CASTLES, 2: Katz et al. (1997), 3: this work, the mid-infrared observation, and 4: this work, the lens model with smooth potential.

TABLE 4
FLUX RATIOS OF Q2237+030

| wavelength | date | B/A | flux ratio C/A | D/A | reference |
|----------------------------|-------------------|-------------------|-------------------|-------------------|-----------|
| C _{III} continuum | 2002.07.16, 17 | 0.200 ± 0.036 | 0.484 ± 0.150 | 0.325 ± 0.091 | 1 |
| Mg _{II} continuum | 2002.07.16, 17 | 0.232 ± 0.042 | 0.406 ± 0.089 | 0.351 ± 0.070 | 1 |
| C _{III} line | 2002.07.16, 17 | 0.492 ± 0.123 | 0.602 ± 0.187 | 0.624 ± 0.175 | 1 |
| Mg _{II} line | 2002.07.16, 17 | 0.505 ± 0.086 | 0.487 ± 0.107 | 0.566 ± 0.113 | 1 |
| H β line | 2002.08.10 | 0.376 ± 0.007 | 0.387 ± 0.007 | 0.461 ± 0.004 | 2 |
| [O _{III}] line | 2002.08.10 | 0.81 ± 0.04 | 0.88 ± 0.05 | 1.09 ± 0.05 | 2 |
| 8.9 & 11.7 μm | 1999.07.28, 09.24 | 1.11 ± 0.11 | 0.59 ± 0.09 | 1.00 ± 0.10 | 3 |
| 11.7 μm | 2000.07.11 | 1.11 ± 0.09 | 0.72 ± 0.07 | 1.17 ± 0.09 | 4 |
| 8 GHz | 1995.06.25 | 1.08 ± 0.27 | 0.55 ± 0.21 | 0.77 ± 0.23 | 5 |
| 11.7 μm | 2005.10.11, 12 | 0.84 ± 0.05 | 0.46 ± 0.02 | 0.87 ± 0.05 | 6 |
| SIE | | 0.867 | 0.457 | 0.855 | 7 |
| SIE+ES | | 0.887 | 0.448 | 0.826 | 7 |

NOTE. — The references are 1: Wayth, O'Dowd & Webster (2005; extinction corrected), 2: Metcalf et al. (2004; with the small aperture in their table 1), 3: Agol et al. (2000), 4: Agol et al. (2001), 5: Falco et al. (1996), 6: this work, the mid-infrared observation, and 7: this work, the lens model with smooth potential.

TABLE 5
BEST MODEL PARAMETERS AND PREDICTED FLUX RATIOS

| model | b ($''$) | (x_0, y_0) ($''$) | e | θ_e (deg) | γ | θ_γ (deg) | N_{dof} | χ^2 | flux ratio | | | μ^a |
|-------------------------|-----------------|--------------------------|-------|---------------------|----------|--------------------------|------------------|----------|------------|-------|-------|---------|
| MG0414+0534 | | | | | | | | | A2/A1 | B/A1 | C/A1 | |
| SIE+ES ^b | 1.174 | (0.449, -1.316) | 0.201 | 34 | 0.121 | -83 | 1 | 297.0 | 1.090 | 0.257 | 0.107 | 60.7 |
| SIE+ES+X ^c | 1.089 | (0.472, -1.273) | 0.199 | -72 | 0.123 | 57 | 0 | 8.6 | 1.063 | 0.321 | 0.158 | 47.0 |
| SIE+ES+Xf ^d | 1.088 | (0.473, -1.273) | 0.200 | -72 | 0.124 | 57 | 3 | 24.5 | 1.063 | 0.323 | 0.158 | 46.7 |
| SIE+ES+Xfp ^e | 1.065 | (0.470, -1.278) | 0.191 | -72 | 0.145 | 57 | 1 | 10.2 | 1.070 | 0.387 | 0.133 | 59.3 |
| Q2237+030 | | | | | | | | | B/A | C/A | D/A | |
| SIE | 0.861 | (0.077, 0.939) | 0.332 | 67 | | | 3 | 17.9 | 0.867 | 0.457 | 0.855 | 16.0 |
| SIE+ES ^b | 0.854 | (0.075, 0.939) | 0.371 | 65 | 0.015 | -47 | 1 | 1.0 | 0.887 | 0.448 | 0.826 | 15.0 |

^aTotal magnification factor of all four images.

^bSIE plus an external shear model.

^cObject X modeled as an SIS with an optimized Einstein angle of $b_X = 0.''187$ is considered at the position of (0.''857, 0.''180) with an error of 0.''010.

^dThe observed mid-infrared flux ratios are also used as constraints.

^eAdditional lens potentials with multipole terms having an angle being aligned with θ_e are considered, given as $|\epsilon_3| = 1.298 \times 10^{-2}$ for $m = 3$ and $|\epsilon_4| = 8.588 \times 10^{-3}$ for $m = 4$. The observed mid-infrared flux ratios are also used as constraints.

the observed mid-infrared flux ratios as constraints (referred to as SIE+ES+Xf in Table 5), which however does not meaningfully improve the model fits: the obtained $\chi^2/N_{\text{dof}} \sim 8.2$ is dominated by the uncertainties in reproducing the flux ratios ($\chi^2/N_{\text{dof}} \sim 5.2$).

We compare the flux ratios predicted by these lens models with the observed ones, especially in the current mid-infrared wavelength of $11.7 \mu\text{m}$ and other radio wavelengths, because the flux ratios in both wavebands are extinction free and microlensing free, and are advantageous to search for millilensing by CDM subhalos (e.g., Kochanek & Dalal 2004). We have found that the mid-infrared flux ratios agree well with the radio flux ratios obtained by Katz, Moore, & Hewitt (1997). However, it is suggested that for MG0414+0534, SIE+ES and even SIE+ES+X do not well reproduce the flux ratio of a brightest image pair A2/A1 in a statistically significant manner, i.e., the observed $A2/A1 \lesssim 0.90$ is systematically smaller than the best prediction of $A2/A1 \simeq 1.063$ by SIE+ES+X. The deviation amounts to about 20 % level, or about 4σ level for the mid-infrared flux ratio and even more for the radio flux ratios. The increase of the mass of object X or the change of its redshift may further reduce A2/A1 to be consistent with the observed ratio, which however leads to larger discrepancy with other flux ratios such as B/A1 and C/A1. It is worth noting here that given a set of best-fit model parameters, the change for one of those within $\Delta\chi^2 \leq 1$ yields the change of flux ratios being only $O(10^{-3})$. Thus, we need to adopt a more complex model in order to explain the observed flux ratios.

To further test the possibility of reproducing A2/A1 for MG0414+0534, we consider the addition of lens potentials with higher order multipoles, $\phi_m = (\epsilon_m r/m) \cos m(\theta - \theta_m)$, to the primary lens model including object X, where r and θ denote a projected radius and angle, respectively, and ϵ_m and θ_m denote the amplitude and orientation angle of ϕ_m , respectively. We confine our attention to $m = 3$ and 4 terms, where θ_m is constrained to be aligned with the ellipsoid ($\theta_m = \theta_e$) as was explored by Kochanek & Dalal (2004). The mid-infrared flux ratios are also used as constraints, so N_{dof} is 1 in this model (referred to as SIE+ES+Xfp in Table 5). Inclusion of such multipoles may be able to reproduce anomalous flux ratios (Evans & Witt 2003). However, the discrepancy with the observed A2/A1 still remains; the predicted ratio A2/A1 of 1.070 from this model is even worse than that without multipoles, 1.063. We thus require an additional lens substructure possibly near these images, whereby their flux ratio is directly modified.

4.1.2. Q2237+030

For the Einstein Cross, an SIE alone reasonably reproduces the image positions ($\chi^2/N_{\text{dof}} \sim 6.0$) and the consideration of an external shear (SIE+ES) yields successful fits ($\chi^2/N_{\text{dof}} \sim 1.0$). These models are also able to reproduce the observed flux ratios in the mid-infrared wavelength (this work; Agol et al. 2000, 2001) and those in the radio wavelength (Falco et al. 1996): the differences between the modeled flux ratios and our mid-infrared flux ratios are confined well within 1σ level. Even if our mid-infrared flux ratios are also used as additional constraints, we obtain the resultant change of χ^2

as only $\Delta\chi^2 \sim 0.4$ for an SIE+ES model, which indicates that the model fitting to the flux ratios is satisfactory. Indeed, many smooth models for this lens system have already been constructed so far, as summarized in Wyithe, Agol, & Fluke (2002), and some of previous models have also reproduced the current mid-infrared flux ratios in a reasonable manner. This suggests that we do not necessarily require an explicit lens substructure for the reproduction of the mid-infrared flux ratios.

4.2. Limits on Substructure Lensing

Within the limitation of our smooth lens models, it is yet unsuccessful to explain the mid-infrared flux ratio of $A2/A1 = 0.90 \pm 0.04$ for MG0414+0534. This appears to be also the case in other, more complicated lens models based on a multipole-Taylor expansion for a lens potential by Trotter, Winn, & Hewitt (2000). They made use of high-resolution, VLBI radio continuum maps, which show the complex spatial structure with multiple components and kinks (Ros et al. 2000). Such detailed features of lensed images are also a possible probe for CDM substructures (Inoue & Chiba 2005a,b; Chen et al. 2007). However Trotter et al.'s model being best fitted to the positions of multiple components of the lensed images does not reproduce the radio flux ratios well. In particular, the suggested flux ratio A2/A1 is systematically larger than unity, contrary to the observed flux ratios (see also Kochanek & Dalal 2004).

In this subsection, we explore the presence of another lens substructure (i.e., other than object X) in the form of a star or a CDM subhalo, which can cause, if being located in the vicinity of the lensed images, the discrepancy between the observed and predicted flux ratios. The mid-infrared flux ratio is particularly useful in this regard, because the size of the corresponding near-infrared emitting region in the rest frame, which corresponds to the innermost dust torus of the lensed QSOs, can be estimated from the luminosity of the central engine. Based on the results of dust reverberation observations (Minezaki et al. 2004; Suganuma et al. 2006), where the lag time between the K -band and UV-optical continuum flux variations is calibrated, the radius of the near-infrared (K -band) emitting region can be estimated as $\log R$ (light days) $= (-2.15 - M_V/5.0) \times c$, where M_V is the absolute magnitude of AGN in V band and c is the light velocity, or R (pc) $= 1.2 \times (\lambda L_\lambda^{\text{opt}}/10^{46} \text{ ergs s}^{-1})^{1/2}$, where $\lambda L_\lambda^{\text{opt}}$ is the optical ($\lambda = 0.51 \mu\text{m}$) luminosity⁸.

Unfortunately, it is difficult to obtain the optical luminosities of MG0414+0534 and Q2237+030 from the fluxes in the rest-frame optical wavelengths. The rest-frame optical flux of MG0414+0534 is affected by large extinction, whose nature is not fully understood (e.g., Angonin-Willaime et al. 1999; Eliasdottir et al. 2006), and that of Q2237+030 is affected by microlensing in addition to extinction (Udalski et al. 2006 and references therein; Eliasdottir et al. 2006). Instead, we estimate their optical luminosities from the mid-infrared fluxes

⁸ In Paper I, the estimation of M_V and resultant size of a torus contained small errors: correctly, the radii of the rest-frame K -band emission region are estimated as $R = 0.4$ pc for PG1115+080 and $R = 2.2$ pc for B1422+231. Other parameters which depend on R change only very slightly, so the conclusion in Paper I remains unchanged.

and the composite SED of QSOs. Although the scatter of the rest-frame optical to near-infrared luminosity ratio is not small, its systematic effect such as the luminosity dependency and the redshift dependency seems to be small (Jiang et al. 2006).

From the mid-infrared fluxes and the composite SED of QSOs presented by Richards et al. (2006), we obtain the optical luminosity of $\lambda L_{\lambda}^{\text{opt}} = 9.8 (\mu/50)^{-1} \times 10^{45} \text{ ergs s}^{-1}$ and $\lambda L_{\lambda}^{\text{opt}} = 6.0 (\mu/15)^{-1} \times 10^{45} \text{ ergs s}^{-1}$ for MG0414+0534 and Q2237+030 respectively, where μ is the magnification factor of the lens model. Based on the dust reverberation, the source radii of the rest-frame K -band emitting region are estimated as $R = 1.2 (\mu/50)^{-1/2} \text{ pc}$ and $R = 0.9 (\mu/15)^{-1/2} \text{ pc}$. In a longer rest-frame wavelength than K band, the radius of a near-infrared emitting region is larger than that at K band, because the cooler dust distributed at larger radii of the dust torus would contribute more to the near-infrared flux. The rest-frame wavelengths of observing $11.7 \mu\text{m}$ emission are $3.2 \mu\text{m}$ for MG0414+0534 and $4.3 \mu\text{m}$ for Q2237+030, then we estimate the source radius as $R_S \sim 2 (\mu/50)^{-1/2} \text{ pc}$ and $R_S \sim 2 (\mu/15)^{-1/2} \text{ pc}$ for MG0414+0534 and Q2237+030, respectively. Their angular sizes are estimated as $\theta_S \sim 3 \times 10^{-4} (\mu/50)^{-1/2} \text{ arcsec}$ and $\theta_S \sim 2 \times 10^{-4} (\mu/15)^{-1/2} \text{ arcsec}$.

To be compared with θ_S is an Einstein angle θ_E provided by either a star with sub-solar mass (microlensing) or a CDM subhalo with $M = 10^{7-9} M_{\odot}$ (millilensing), which causes anomaly in the flux ratios of lensed images (Wyithe et al. 2002; Paper I). Denoting M_E as a substructure mass inside θ_E , the latter is expressed as $\theta_E = 5 \times 10^{-7} (M_E/0.1 M_{\odot})^{1/2} \text{ arcsec}$ for MG0414+0534 and $\theta_E = 2 \times 10^{-6} (M_E/0.1 M_{\odot})^{1/2} \text{ arcsec}$ for Q2237+030. As a reference for a spatially extended substructure being applicable to a CDM subhalo, we use an SIS. For its mass indicator, we use M_{100}^{SIS} that is defined as the mass within a radius of 100 pc from the center of an SIS. As shown in Paper I, an SIS having a circular velocity of V_c provides an Einstein radius of $\theta_E \propto V_c^2$, while $V_c^2 \propto M_{100}^{\text{SIS}}$ for a given radius of 100 pc. We then obtain $\theta_E = 3 \times 10^{-4} (M_{100}^{\text{SIS}}/10^6 M_{\odot}) \text{ arcsec}$ for MG0414+0534 and $\theta_E = 6 \times 10^{-4} (M_{100}^{\text{SIS}}/10^6 M_{\odot}) \text{ arcsec}$ for Q2237+030.

Comparison between θ_E and θ_S indicates that a star with sub-solar mass is unable to magnify mid-infrared flux arisen from a dust torus, because $\theta_E \ll \theta_S$ (or $\theta_E < \theta_S/10$, see Wyithe et al. 2002 for this argument). For Q2237+030, the agreement between the observed mid-infrared flux ratios and the predicted ones by a smooth lens model suggests $\theta_E < \theta_S/10$, which yields $M_E < 8(\mu/15)^{-1} M_{\odot}$ or $M_E < 8 M_{\odot}$ using an SIE+ES smooth model with $\mu = 15.0$ (Table 5). Thus, the reported anomalous flux ratios in the optical bands are caused by microlensing by a star (Schneider et al. 1988; Irwin et al. 1989), not by millilensing of a CDM subhalo. For MG0414+0534, both of the radio and mid-infrared flux ratios appear to be modified by substructure lensing compared with the prediction of a smooth lens model; the difference in the most problematic flux ratio, A2/A1, is at most about 20 %. Taking into account θ_S of a dust torus, the change of a flux ratio by at most about 20 % from a smooth-lens prediction can be caused by a substructure with $\theta_E \simeq \theta_S/10$ if its position is just

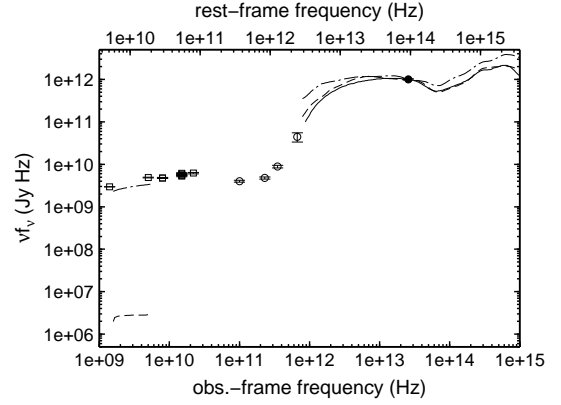


FIG. 3.— The spectral energy distribution (SED) of MG0414+0534 from infrared to radio wavelength. The filled circle is the $11.7 \mu\text{m}$ flux obtained by this work. The open circles are the sub-mm fluxes taken from Barvainis & Ivison (2002), and the open boxes are the radio continuum fluxes taken from Katz et al. (1997). The solid line is the composite SED of QSOs by Richards et al. (2006), the dashed and dash-dotted lines are, respectively, the mean energy distributions (MEDs) of radio-quiet and radio-loud QSOs by Elvis et al. (1994).

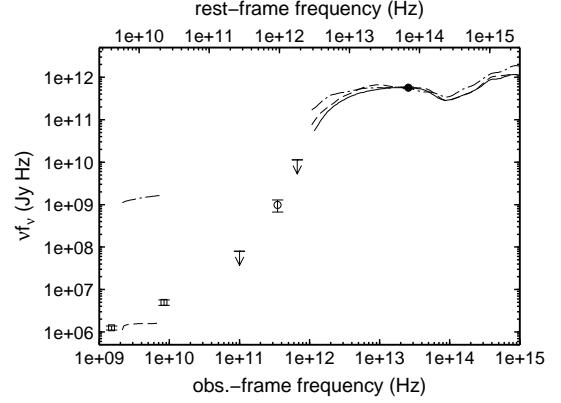


FIG. 4.— The SED of Q2237+030 from infrared to radio wavelength. The filled circle is the $11.7 \mu\text{m}$ flux obtained by this work. The open circle and the upper limits are the sub-mm fluxes taken from Barvainis & Ivison (2002), and the open boxes are the radio continuum fluxes taken from Falco et al. (1996). The solid line is the composite SED of QSOs by Richards et al. (2006), the dashed and dash-dotted lines are, respectively, the MEDs of radio-quiet and radio-loud QSOs by Elvis et al. (1994).

centered at either of the lensed image A2 or A1 (Inoue & Chiba 2005b); a more massive substructure located outside the image can give rise to the same amount of a flux perturbation. Thus, we obtain a lower limit on M_E , namely, $M_E \gtrsim 340(\mu/50)^{-1} M_{\odot}$ inside an Einstein angle (i.e., $M_E \gtrsim 360 M_{\odot}$ for an SIE+ES+X model with $\mu = 47.0$), thereby suggesting a CDM subhalo is likely to affect the mid-infrared flux ratio. If it is modeled as an SIS, we obtain $M_{100}^{\text{SIS}} \gtrsim 9.7 \times 10^4 (\mu/50)^{-1/2} M_{\odot}$ inside radius of 100 pc (i.e., $M_{100}^{\text{SIS}} \gtrsim 1.0 \times 10^5 M_{\odot}$ for an SIE+ES+X smooth model).

4.3. Other Possible Mid-Infrared Sources

Although infrared flux of AGN is dominated by thermal emission of the dust torus, a minor fraction might be contributed by other sources, such as an extension of op-

tical continuum emission from the accretion disk (Kishimoto, Antonucci, & Blaes 2005; Tomita et al. 2006; Minezaki et al. 2006), non-thermal emission from a compact region relating to radio activity (Neugebauer & Matthews 1999; Enya et al. 2002), or infrared emission from starburst activity, which is suggested for some high redshift QSOs (Carilli et al. 2001; Omont et al. 2001). Since the former two sources are more compact than the dust torus while the latter is more spatially extended, possible contributions of both of them to the mid-infrared flux might have an influence on the estimation of the limits on the substructure. We will examine their possible contributions.

The source size of the accretion disk is so small that the flux originated from it could be affected by microlensing. However, the mid-infrared flux ratios of both of MG0414+0534 and Q2237+030 are considered not to be affected by the microlensing of the accretion disk component. Firstly, the mid-infrared flux ratios and the radio flux ratios of MG0414+0534 are in good agreement with each other. The source size of the radio emission is also considered to be so large that its flux would not be affected by microlensing (e.g., Kochanek & Dalal 2004), and the agreement with both flux ratios suggests that the mid-infrared flux ratios of MG0414+0534 are not affected by microlensing. Secondly, possible time variation of mid-infrared flux ratios of Q2237+030 at an interval of 5–6 years are examined by comparing Agol et al. (2000, 2001) with this work. We found that the mid-infrared flux ratios are almost constant, or the small change between them shows an opposite trend to that observed in the optical flux ratios that are heavily affected and changed by microlensing (see Section 4.4 for detail). The mid-infrared flux ratios of Q2237+030 obtained in different epochs of observations suggest that they are also not affected by microlensing.

The contribution of non-thermal emission to the mid-infrared flux is estimated based on the SEDs of MG0414+0534 and Q2237+030 from infrared to radio wavelengths. Their SEDs are presented in Figure 3 and Figure 4. The filled circles in the figures are the 11.7 μm flux obtained by this work. The open circles and the upper limits are the sub-mm fluxes taken from Barvainis & Ivison (2002), and the open boxes are the radio continuum fluxes taken from Katz et al. (1997) for MG0414+0534 and Falco et al. (1996) for Q2237+030, respectively. The solid line is the composite SED of QSOs by Richards et al. (2006), the dashed line and the dash-dotted lines are the mean energy distribution (MED) of radio-quiet QSOs and radio-loud QSOs by Elvis et al. (1994). Those composite SEDs of QSOs are normalized at the 11.7 μm fluxes. As presented in Figure 3 and Figure 4 respectively, the infrared to radio SED of MG0414+0534 agrees with the typical SED of radio-loud QSOs, while that of Q2237+030 agrees with the typical SED of radio-quiet QSOs.

It is generally accepted that the infrared emission ($\sim 10^{11.5-14.5}$ Hz) of QSOs is dominated by thermal reradiation of dust torus heated by UV radiation from the accretion disk, while the radio emission ($\lesssim 10^{11.5}$ Hz) of QSOs is non-thermal in origin, synchrotron radiation from relativistic jet. Since the radio continuum emission of MG0414+0534 obtained by Katz et al. (1997) follows a power-law SED, the contribution of non-thermal

emission to the mid-infrared flux of MG0414+0534 is estimated by simply extrapolating the power-law SED of the radio continuum emission to the mid-infrared wavelength. Although MG0414+0534 is a radio-loud QSO, it is estimated to less than $\sim 5\%$, and moreover, it would be smaller than this estimation, because the power-law SED by synchrotron radiation would have a break at some frequency higher than the radio wavebands. The radio to mid-infrared flux ratio of Q2237+030 is about 3 order of magnitudes smaller than that of MG0414+0534 as presented in Figure 3 and Figure 4, thus the contribution of non-thermal emission to the mid-infrared flux of Q2237+030 is expected to be quite small. Therefore, the possible non-thermal emission in the mid-infrared flux would have little effect on the discussion of substructure lensing for both targets.

In addition to AGN activity, starburst activity is known to be another important source for powerful far-infrared emission of galaxies (e.g. Sanders & Mirabel 1996). Carilli et al. (2001) and Omont et al. (2001) carried out observations at 250 GHz (1.2 mm) of a total of ~ 100 high redshift ($z \gtrsim 4$) QSOs. About one third of them were detected at 250 GHz, which showed excess emission over the composite SED of low-redshift radio-quiet QSOs in rest-frame far-infrared wavelength. They suggested that substantial fraction of the far-infrared luminosity arises from starburst activity, although they could not exclude the possibility of its AGN origin. Thus, starburst activity associated with QSOs could be assessed by the excess emission in far-infrared wavelength. As presented in Figure 3 and Figure 4, the far-infrared fluxes of MG0414+0534 and Q2237+030 fall at the MED (and its interpolation at far-infrared to sub-mm wavelengths) of radio-quiet QSOs normalized by their mid-infrared fluxes, and no excess emission in far-infrared is detected. Therefore, they do not host significant starburst, and the contribution of starburst activity would be unimportant.

4.4. Comparison with Other Observations of Q2237+030

The mid-infrared flux ratios of Q2237+030 obtained by Agol et al. (2000, 2001) and those of this work are almost the same within the errors. However, the flux ratio of image A is different from Agol et al. (2001; $f(A)/f(\text{total}) = 0.250 \pm 0.015$) and this work ($f(A)/f(\text{total}) = 0.315 \pm 0.005$) at about 4σ level, and sorting the images in order of brightness, $f(B) \approx f(D) \gtrsim f(A) > f(C)$ by Agol et al. (2001) while $f(A) \gtrsim f(B) \approx f(D) > f(C)$ by this work. We will discuss this difference, which would suggest a time variation of the mid-infrared flux ratios at an interval of five years.

First, we argue that the intrinsic variation of QSO and the time delay between the lensed images cannot explain the difference of the mid-infrared flux ratios between the two observations. That is because the lens models for Q2237+030 yield the time delays between the images as less than a day (e.g., Schneider et al. 1988; Rix et al. 1992; Wambsganss & Paczynski 1994) and they are very short compared to the timescale of flux variation of QSOs.

If the contribution to the mid-infrared flux originated from compact regions like the accretion disk is large, the mid-infrared flux and flux ratio can show time variation

due to microlensing, in a similar way to the optical flux and flux ratios. However, according to the optical light curves presented in Udalski et al. (2006), the optical flux of image B relative to the others' fluxes at the observation date of Agol et al. (2001) was fainter than that at the date of this observation. This is an opposite trend to the changes in the mid-infrared flux ratios. Therefore, the microlensing of the compact source cannot explain the difference of the mid-infrared flux ratios between the two observations. Thus, the origin of the discrepancy remains unknown.

As shown in Table 4, a notable difference between the narrow line region (NLR) $[O_{III}]$ and the mid-infrared flux ratios of Q2237+030, especially for C/A, also needs to be understood (Metcalf et al. 2004). This can be explained as follows. The first possibility is that the NLR is so large that some of the flux of image A or D could leak out of the aperture to image C, causing the high C-to-A magnification ratio for $[O_{III}]$. The second possibility is that the NLR has a complex shape with a non-uniform emissivity profile so that the total magnification differs from that of the smaller mid-infrared emission (Yonehara 2006). For instance, a double corn-like structure in the NLR could account for the observed double peaks in image A in $[O_{III}]$. We note that if any substructures (as suggested by Metcalf et al. 2004) are present in Q2237+030, their impact on the mid-infrared flux remains minor because our lens model with a smooth potential (SIE+ES) successfully reproduces the mid-infrared flux ratios as well as the image positions.

5. CONCLUSION

We have presented mid-infrared imaging at $11.7 \mu\text{m}$ for the quadruple lens systems, MG0414+0534 and Q2237+030. The lensed images of these QSOs have

successfully been separated from each other owing to the diffraction-limited resolution of the COMICS/Subaru images with $\text{FWHM} = 0.''33$. Our calibration of the mid-infrared fluxes and flux ratios for different lensed images have revealed that (1) the mid-infrared flux ratio A2/A1 of MG0414+0534 shows a statistically significant deviation from the prediction of a smooth lens model, which is comprised of an SIE plus an external shear and a possibly faint satellite, object X, and that (2) the mid-infrared flux ratios between all the four images of Q2237+030 are in good agreement with the prediction of a smooth lens model. These results, combined with the estimated dimensions of dust tori around these QSOs based on the relation of dust reverberation mapping, set limits on the mass of a lens substructure, which is responsible for the anomalous flux ratios. For MG0414+0534, the mass of a supposed substructure inside an Einstein radius, is $M_E \gtrsim 360M_\odot$, thus indicating that a CDM subhalo is most likely affecting the mid-infrared flux ratio. If it is an SIS, the mass inside radius of 100 pc is given as $\gtrsim 1.0 \times 10^5 M_\odot$. For Q2237+030, assuming a smooth lens potential, the observed mid-infrared magnification flux ratios suggest $M_E < 8M_\odot$. Thus, we conclude that the optical anomalous flux ratios and the time variations are entirely due to microlensing by stars, in agreement with Agol et al. (2000).

We thank Takuya Fujiyoshi for his expert assistance during our observing runs with COMICS/Subaru. This work has been supported in part by a Grant-in-Aid for Scientific Research (17540210, 20340039) of the Ministry of Education, Culture, Sports, Science and Technology in Japan.

REFERENCES

- Agol, E., Jones, B., & Blaes, O. 2000, *ApJ*, 545, 657
 Agol, E., Wyithe, S., Jones, B., & Fluke, C. 2001, *PASA*, 18, 166
 Angonin-Willaime, M.-C., Vanderriest, C., Courbin, F., Burud, I., Magain, P., & Rigaut, F. 1999, *A&A*, 347, 434
 Barvainis, R., & Ivison, R. 2002, *ApJ*, 571, 712
 Carilli, C. L. et al. 2001, *ApJ*, 555, 625
 Chen, J., Rozo, E., Dalal, N., & Taylor, J. E. 2007 *ApJ*, 659, 52
 Chiba, M. 2002, *ApJ*, 565, 17
 Chiba, M., Minezaki, T., Kashikawa, N., Kataza, H., & Inoue, K. T. 2005, *ApJ*, 627, 53 (Paper I)
 Cohen, M., Walker, R. G., Carter, B., Hammersley, P., Kidger, M., & Noguchi, K. 1999, *AJ*, 117, 1864
 Diemand, J., Kuhlen, M., & Madau, P. 2007, *ApJ*, 657, 262
 Eliasdottir, A., Hjorth, J., Toft, S., Burud, I., & Paraficz, D. 2006, *ApJS*, 166, 443
 Elvis, M. et al. 1994, *ApJS*, 95, 1
 Enya, K., Yoshii, Y., Kobayashi, Y., Minezaki, T., Suganuma, M., Tomita, H., & Peterson, B. A. 2002, *ApJS*, 141, 45
 Evans, N. W., & Witt, H. J. 2003, *MNRAS*, 345, 1351
 Falco, E. E., Lehar, J., Perley, R. A., Wambsganss, J., & Gorenstein, M. V. 1996, *AJ*, 112, 897
 Falco, E. E., Lehar, J., & Shapiro, I. I. 1997, *AJ*, 113, 540
 Hewitt, J. N., Turner, E. L., Lawrence, C. R., Schneider, D. P., & Brody, J. P. 1992, *AJ*, 104, 968
 Huchra, J., et al. 1985, *AJ*, 90, 691
 Inoue, K. T., & Chiba, M. 2003, *ApJ*, 591, L83
 Inoue, K. T., & Chiba, M. 2005, *ApJ*, 633, 23
 Inoue, K. T., & Chiba, M. 2005, *ApJ*, 634, 77
 Irwin, M. J., Webster, R. L., Hewett, P. C., Corrigan, R. T., & Jedrzejewski, R. I. 1989, *AJ*, 98, 1989
 Jiang, L. et al. 2006, *AJ*, 132, 2127
 Kataza, H. et al. 2000, *Proc. SPIE Vol. 4008*, p. 1144-1152, *Optical and IR Telescope Instrumentation and Detectors*, Masanori Iye; Alan F. Moorwood; Eds.
 Katz, C. A., Moore, C. B., & Hewitt, J. N. 1997, *ApJ*, 475, 512
 Keeton, C. R. 2001, preprint (astro-ph/0102340)
 Kishimoto, M., Antonucci, R., & Blaes, O. 2005, *MNRAS*, 364, 640
 Klypin, A., Kravtsov, A. V., Valenzuela, O., & Prada, F. 1999, *ApJ*, 522, 82
 Kochanek, C. S., & Dalal, N. 2004, *ApJ*, 610, 69
 Kormann, R., Schneider, P., & Bartelmann, M. 1994, *A&A*, 284, 285
 Lawrence, C. R., Elston, R., Januzzi, B. T., & Turner, E. L. 1995, *AJ*, 110, 2570
 Malhotra, S., Rhoads, J. E., & Turner, E. L., 1997, *MNRAS*, 288, 138
 McLeod, B. A., Bernstein, G. M., Rieke, M. J., & Weedman, D. W. 1998, *AJ*, 115, 1377
 Metcalf, R. B., & Madau, P. 2001, *ApJ*, 563, 9
 Metcalf, R. B. 2002, *ApJ*, 580, 696
 Metcalf, R. B., Moustakas, L. A., Bunker, A. J., & Parry, I. R. 2004, *ApJ*, 607, 43
 Minezaki, T. et al. 2004, *ApJ*, 600, L35
 Minezaki, T. et al. 2006, *ApJ*, 643, L5
 Moore, B., Ghigna, S., Governato, F., Lake, G., Quinn, T., & Stadel, J. 1999, *ApJ*, 524, L19
 Neugebauer, G., & Matthews, K. 1999, *AJ*, 118, 35
 Omont, A. et al. 2001, *A&A*, 374, 371
 Richards, G. T. et al. 2006, *ApJS*, 166, 470
 Rix, H.-W., Schneider, D. P., & Bahcall, J. N. 1992, *AJ*, 104, 959
 Ros, E. et al. 2000, *A&A*, 362, 845
 anders, D. B., & Mirabel, I. F. 1996, *ARA&A*, 34, 749
 Schechter, P. L., & Moore, C. B. 1993, *AJ*, 105, 1

- Schneider, D. P., Turner, E. L., Gunn, J. E., Hewitt, J. N., Schmidt, M., & Lawrence, C. R. 1988, *AJ*, 95, 1619
- Suganuma, M. et al. 2006, *ApJ*, 639, 46
- Tomita, H. et al. 2006, *ApJ*, 652, L13
- Tonry, J. L., & Kochanek, C. S., 1999, *AJ*, 117, 2034
- Trotter, C. S., Winn, J. N., & Hewitt, J. N. 2000, *ApJ*, 535, 671
- Udalski, A. et al. 2006, *Acta Astronomica*, 56, 293 (astro-ph/0701300)
- Wambsganss, J., & Paczynski, B. 1994, *AJ*, 108, 1156
- Wayth, R. B., O'Dowd, M., & Webster, R. L. 2005, *MNRAS*, 359, 561
- Wyithe, J. S. B., Agol, E., & Fluke, C. J. 2002, *MNRAS*, 331, 1041
- Yonehara, A. 2008, *ApJ*, 646, 16